

ARTICLE



Dual roles for LUBAC signaling in thymic epithelial cell development and survival

Reema Jain^{1,2,5}, Kelin Zhao^{1,2}, Julie M. Sheridan^{1,2}, Melanie Heinlein^{1,2,6}, Fiona Kupresanin^{1,7}, Waruni Abeysekera^{1,2}, Cathrine Hall^{1,2}, James Rickard^{1,2}, Philippe Bouillet^{1,2}, Henning Walczak^{3,4}, Andreas Strasser^{1,2}, John Silke^{1,2} and Daniel H. D. Gray^{1,2}✉

© The Author(s), under exclusive licence to ADMC Associazione Differenziamento e Morte Cellulare 2021

Thymic epithelial cells (TECs) form a unique microenvironment that orchestrates T cell differentiation and immunological tolerance. Despite the importance of TECs for adaptive immunity, there is an incomplete understanding of the signalling networks that support their differentiation and survival. We report that the linear ubiquitin chain assembly complex (LUBAC) is essential for medullary TEC (mTEC) differentiation, cortical TEC survival and prevention of premature thymic atrophy. TEC-specific loss of LUBAC proteins, HOIL-1 or HOIP, severely impaired expansion of the thymic medulla and AIRE-expressing cells. Furthermore, HOIL-1 deficiency caused early thymic atrophy due to Caspase-8/MLKL-dependent apoptosis/necroptosis of cortical TECs. By contrast, deficiency in the LUBAC component, SHARPIN, caused relatively mild defects only in mTECs. These distinct roles for LUBAC components in TECs correlate with their function in linear ubiquitination, NF- κ B activation and cell survival. Thus, our findings reveal dual roles for LUBAC signaling in TEC differentiation and survival.

Cell Death & Differentiation (2021) 28:2946–2956; <https://doi.org/10.1038/s41418-021-00850-8>

INTRODUCTION

The differentiation of haematopoietic progenitors into naive T cells in the thymus is governed by thymic epithelial cells (TECs). Specialized TEC subtypes direct distinct quality control processes in thymocyte differentiation. Cortical thymic epithelial cells (cTECs) mediate early events, including T cell lineage commitment, proliferation, and positive selection of cells expressing TCRs capable of interacting with self-peptide/MHC complexes [1]. By contrast, medullary thymic epithelial cells (mTECs) are important for thymic negative selection and the generation of FOXP3⁺ regulatory T (Treg) cells, thus limiting the risk of autoimmunity [2]. Medullary TECs are uniquely adapted for the induction of immunological tolerance because they express thousands of tissue-specific antigens that greatly increase the scope of thymic negative selection. This property is mediated in mTEC subtypes by the transcriptional regulators AIRE and FEZF2 [2, 3]. These essential functions of TEC in immunity and tolerance have generated considerable interest in the molecular mechanisms of their differentiation and maintenance.

Members of the tumor necrosis factor (TNF) and TNF receptor (TNFR) superfamilies (i.e. the TNFSF and TNFRSF) and NF- κ B transcription factors are critical for TEC differentiation and the establishment of thymic tolerance [4]. Signaling through RANK is required for mTECs during development, whereas signals from other TNFRSF members coordinate the maintenance of postnatal mTECs [5, 6]. Ligation of the TNFRSF members CD40, RANK, and lymphotoxin beta receptor (LT β R) is required for the development of the key

tolerogenic mTEC populations, such as AIRE^{POS} and FEZF2^{POS} cells [3, 5, 7–9]. Yet, precisely how these signals are integrated to direct TEC fate, function and survival remain poorly understood.

LUBAC is a component of TNFR1 and CD40 receptor signaling complexes [10, 11] that attaches linear ubiquitin chains to signal transducers and/or regulators of the canonical NF- κ B pathway, including RIPK1, TRADD, NEMO, and TNFR1 itself [10, 12, 13]. LUBAC is a ~600 kD ubiquitin E3 complex composed of three proteins: SHANK-associated RH domain interacting protein (SIP1/SHARPIN), C3HC4-type zinc finger containing 1 (RBCK1/HOIL-1), and the catalytic component, ring finger protein 31 (RNF31/HOIP) [10, 12, 14–16]. Mutations of these LUBAC components perturb innate and adaptive immune responses [10, 17, 18]. Patients with loss-of-function mutations in HOIL-1 or HOIP were found to be T cell-deficient and (in one patient) had greatly reduced T-cell receptor excision circles, indicating impaired thymic function [17, 18].

There is a differential requirement for HOIP, HOIL-1, and SHARPIN for LUBAC function, signal transduction, differentiation, and cell death. Deficiency in HOIP or HOIL-1 completely abolishes LUBAC activity, impairs NF- κ B activation, and promotes cell death [10, 15, 19–21]. By contrast, SHARPIN-deficient cells can carry out diminished linear ubiquitination via HOIL-1/HOIP complexes, attenuated activation of NF- κ B and JNK signaling pathways, and are also sensitized to cell death [10, 21–23]. Importantly, LUBAC functions in NF- κ B activation and cell survival can be independent [24].

The in vivo consequences of these defects vary according to cell type and developmental context. Complete HOIP- or

¹Walter and Eliza Hall Institute of Medical Research, Melbourne, VIC, Australia. ²Department of Medical Biology, University of Melbourne, Melbourne, VIC, Australia. ³Centre for Cell Death, Cancer and Inflammation, UCL Cancer Institute, University College London, London, UK. ⁴Centre for Biochemistry, University of Cologne, Cologne, Germany. ⁵Present address: Fred Hutchinson Cancer Research Center, Seattle, WA, USA. ⁶Present address: Department of Molecular Oncology, Genentech, Inc., South San Francisco, CA, USA. ⁷Present address: ANZAC Research Institute, Concord, Australia. ✉email: dgray@wehi.edu.au

Edited by G. Melino

Received: 17 February 2021 Revised: 26 July 2021 Accepted: 2 August 2021

Published online: 11 August 2021

HOIL-1-deficiency causes embryonic lethality due to TNF-induced vascular defects [21, 25]. The loss-of-function SHARPIN mutant mice, *cpdm*, are viable but succumb to severe dermatitis from approximately six weeks of age [26, 27], primarily due to sensitization to TNF-induced cell death via apoptosis or necroptosis [10, 21–23]. Roles for LUBAC in lymphocyte differentiation, activation, and survival (e.g., [20, 28, 29]) have also been reported. Key questions in the field remain how complete or partial loss of LUBAC function impacts various tissues and how these defects influence inflammatory and immune pathology [17, 18].

Given the importance of TNFRSF signaling in TEC and thymic tolerance [7, 9, 30, 31], we investigated whether LUBAC function was required for TEC development and homeostasis. Conditional ablation of HOIP or HOIL-1 in TEC caused severe thymic atrophy and T cell deficiency. HOIL-1 was required for the development of the thymic medulla in young mice and the maintenance of cTEC in adults. Thymic atrophy and the demise of HOIL-1-deficient TECs were driven in part by caspase-8/MLKL-driven apoptosis/necroptosis; blockade of this process restored cortical and medullary microenvironments and thymic T cell production. Conversely, only mild disruption of the thymic microenvironment was observed in SHARPIN-deficient mice, confined to a defect in immature mTECs that was not related to cell death. These findings identify LUBAC as an essential signaling hub with distinct roles in mTEC development, cTEC survival, and thymic function.

RESULTS

LUBAC proteins HOIL-1 and HOIP in TECs are essential to maintain thymic function

We first assessed expression of the three LUBAC components in RNAseq data from TEC subpopulations purified from young adult 8 week-old mice. TEC can be sub-divided into three main populations: cTEC, MHC II^{low} mTEC (termed mTEC^{low}) that contain a mixture of precursors and differentiated cells, and MHC II^{high} mTEC (termed mTEC^{high}) including cycling cells and the AIRE⁺ subset [30]. All three known LUBAC components were transcribed in all TEC subsets, with *Rnf31* (encoding HOIP) relatively lower in mTEC^{high}, while mTEC^{low} expressed the highest levels of *Sip1* (encoding SHARPIN) (Fig. 1A). To determine the roles of LUBAC components in TECs in vivo, we generated mice with *Foxn1*^{Cre}-driven deletion of *Rbck1* or *Rnf31*, hereafter termed *Hoil-1*^{ΔFoxn1} and *Hoip*^{ΔFoxn1}, respectively [20, 21, 25] (specific deletion confirmed in Figure S1A). Mice in both of these strains were viable, reproduced normally, and had no overt health problems. The role of SHARPIN in TEC development was assessed in the spontaneous loss-of-function mutant *cpdm* mouse strain (*Sh*^{cpdm/cpdm}) [26, 27], prior to the onset of inflammation. We observed a modest reduction in the thymic cellularity of *Sh*^{cpdm/cpdm} mice; however, TEC-specific loss of HOIL-1 or HOIP caused severe thymic atrophy in adult mice (Fig. 1B).

We tracked thymocyte differentiation *Hoil-1*^{ΔFoxn1} mice by analyzing CD4 vs. CD8 expression and observed loss in all major stages of T cell differentiation (Fig. 1C, Fig. S1B). Deeper analysis of

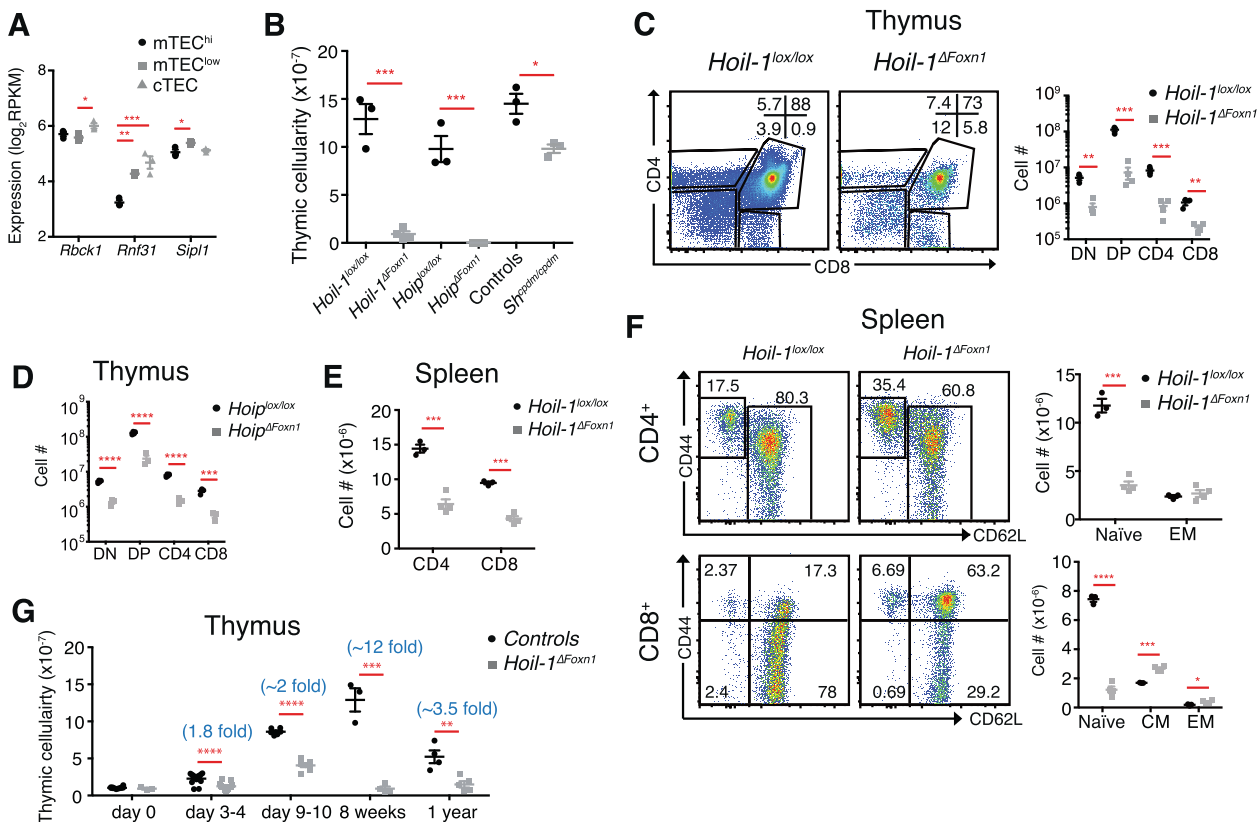


Fig. 1 Early thymic atrophy and T cell defects in *Hoil-1*^{ΔFoxn1} and *Hoip*^{ΔFoxn1} mice. **A** RNA-seq expression analysis of LUBAC components from cTECs, mTEC^{hi}, and mTEC^{low} from 8-week-old WT mice. **B** Thymic cellularity of 8-week-old *Hoil-1*^{ΔFoxn1} or *Hoip*^{ΔFoxn1}, 6-week-old *Sh*^{cpdm/cpdm} mice versus controls. **C** Flow cytometry plots of thymocyte CD4 vs. CD8 expression from 8-week-old *Hoil-1*^{ΔFoxn1} mice and *Hoil-1*^{lox/lox} controls, with cell numbers quantified (left panel). **D** Thymocyte subset numbers in 3-week-old *Hoip*^{lox/lox} and *Hoip*^{ΔFoxn1} mice. **E** Numbers of splenic TCRβ⁺CD4⁺ and TCRβ⁺CD8⁺ T cells from 8-week-old *Hoil-1*^{ΔFoxn1} and *Hoil-1*^{lox/lox} mice. **F** Flow cytometry plots of CD44 vs. CD62L expression gated on splenic TCRβ⁺CD4⁺ or TCRβ⁺CD8⁺ T cells from eight-week-old *Hoil-1*^{ΔFoxn1} mice and *Hoil-1*^{lox/lox} controls. Graphs show the numbers of naïve (CD44^{low}/CD62L^{high}), effector (CD44^{high}/CD62L^{low}) and central memory (CD44^{high}/CD62L^{high}) T cells. **G** Thymic cellularity of control and *Hoil-1*^{ΔFoxn1} mice at the indicated ages. The numbers in parentheses indicate the mean fold-change in thymic cellularity (controls vs. *Hoil-1*^{ΔFoxn1} mice). All data are representative of at least two independent experiments shown (except **A**) ($n \geq 3$ /group). Graphs show mean \pm SEM and groups were compared with a Student's *t*-test (two-sided, unpaired). * $p < 0.05$, ** $p < 0.01$, *** $p < 0.001$, **** $p < 0.0001$.

CD4⁻CD8⁻ double negative (DN) precursor stages revealed a proportional block at the DN3 stage of differentiation and numerical loss in all thymocyte precursor stages in *Hoil-1^{ΔFoxn1}* mice (Figure S1C). Thymic Treg cell production in 8-week-old *Hoil-1^{ΔFoxn1}* mice was virtually extinguished in the severely atrophic thymi (Fig. S1D). These data show that TEC-specific HOIL-1 deletion led to severe thymic hypotrophy and markedly impaired T cell differentiation.

We then compared the thymic phenotype of young (Fig. 1D) and young adult *Hoip^{ΔFoxn1}* mice (Fig. S1E–G) and found that they closely resembled that of *Hoil-1^{ΔFoxn1}* mice, with severe deficiency in all major thymocyte subsets. Thus, HOIP and HOIL-1 are critical in TECs for establishing or maintaining thymic function, consistent with the essential roles of these proteins in LUBAC activity [21].

The thymic defects in adult *Hoil-1^{ΔFoxn1}* mice caused T cell lymphopenia in peripheral lymphoid tissues (Figure S2A). Both CD4⁺ and CD8⁺ T cells were diminished and, consistent with the thymic atrophy, naïve CD44^{low} CD62L^{high} populations were particularly affected with homeostatic expansion of CD122⁺ “virtual” memory cells (Fig. 1E, F, Figure S2B, C). Although the proportions of proliferating Ki67⁺ T cells and FOXP3⁺ Treg cells were increased in eight-week-old *Hoil-1^{ΔFoxn1}* mice, the overall numbers were largely normal (Figure S2D, E). This loss of naïve T cell populations yet maintenance of the virtual memory and regulatory subsets is consistent with the greater reliance on thymic output of the former [32]. These defects extended to the TCR repertoire, with alterations in T cells expressing distinct TCRβ chains (Figure S2F).

We then assayed thymus size throughout ontogeny to determine whether HOIL-1 was required in TECs for thymic development or homeostasis. Overall thymic cellularity immediately following birth was normal in *Hoil-1^{ΔFoxn1}* mice but by day 3–4 mild thymic hypotrophy was evident (Fig. 1G). All major thymocyte subsets, including Treg cells, were diminished and DN1 and DN3 precursor populations were reduced in four-day-old *Hoil-1^{ΔFoxn1}* mice (Figure S3A–C). T cell lymphopenia was not yet evident in the spleen, although a mild reduction in the proportion of naïve CD4⁺ T cells was detected in four-day-old *Hoil-1^{ΔFoxn1}* mice (Figure S3D–F). Thymus size in *Hoil-1^{ΔFoxn1}* mice peaked at days 9–10 but then atrophied, with approximately 12-fold lower thymic cellularity at eight weeks of age compared to controls (Fig. 1G). These data reveal a differential requirement for LUBAC components in TEC maintenance, with HOIL-1 and HOIP essential for thymic function beyond the perinatal stage and the establishment of a normal naïve T cell pool.

TECs require HOIL-1 or HOIP for their homeostasis

We next investigated the role of HOIL-1 or HOIP in TEC homeostasis at key time points. Low numbers of TECs could be recovered from the atrophied thymi of aged-matched 13-week-old *Hoil-1^{ΔFoxn1}* (Fig. 2A) and *Hoip^{ΔFoxn1}* mice (Fig. 2B). We analysed the phenotype of those TECs that could be recovered and found very similar profiles in both *Hoil-1^{ΔFoxn1}* or *Hoip^{ΔFoxn1}* mice, with severe loss in the number of mTEC (Ly51⁻UEA-1⁺) (Fig. 2C–F). Examination of the thymic architecture of 8-week-old *Hoil-1^{ΔFoxn1}* or *Hoip^{ΔFoxn1}* mice revealed extensive disruption of cortical and medullary regions (labeled with anti-keratin-8 versus anti-keratin-5/UEA-1), including the AIRE⁺ compartment, which had almost disappeared (Fig. 2G–L). The loss of TEC in adult *Hoil-1^{ΔFoxn1}* and *Hoip^{ΔFoxn1}* mice was characterized by large epithelial cell free areas and prominent ERTR7⁺ fibroblastic remodeling (Fig. 2G–L). These data indicate that HOIL-1 and HOIP are required for the differentiation and/or homeostasis of all major TEC subpopulations in the adult thymus. The identical impact of TEC-specific HOIL-1- or HOIP-deficiency on the thymus and TEC phenotype is consistent with observations in other tissues and the complete ablation of LUBAC-mediated linear ubiquitination caused by loss of either protein [10, 15, 21].

We next sought to distinguish whether LUBAC activity was required for TEC differentiation or homeostasis. We assayed TEC composition during the development of *Hoil-1^{ΔFoxn1}* mice and observed a slight reduction in total TEC numbers as early as E15.5 that worsened in 4-day postnatal mice (Fig. 3A). Flow cytometric analysis was used to quantify the major subpopulations of EpCAM⁺ TECs: cTEC and mTEC, and the mTEC subpopulations mTEC^{high} (Ly51⁻UEA-1⁺MHCII⁺CD80^{high}) and mTEC^{low} (Ly51⁻UEA-1⁺MHCII⁺CD80^{low/-}) cells that become apparent in day 4 mice (Fig. 3B–D). We found a severe deficit in mTEC in embryonic and neonatal thymi from *Hoil-1^{ΔFoxn1}* mice (Fig. 3B–D), including the tolerogenic AIRE⁺ population (Fig. 3E). The proportion of Ki67⁺ TECs was increased in E15.5 and day 4 *Hoil-1^{ΔFoxn1}* mice, suggesting specific loss of non-proliferating TECs and/or compensatory proliferation of remaining cells (Fig. 3F, G). Therefore, although TECs from *Hoil-1^{ΔFoxn1}* mice were capable of proliferation and differentiation into the major TEC subpopulations, they were unable to maintain normal numbers. By contrast, relatively normal numbers of cTECs were recovered at these stages (Fig. 3C, D).

The thymic architecture of neonatal *Hoil-1^{ΔFoxn1}* mice was also perturbed. Although the distribution of ERTR7⁺ fibroblasts was comparable, medullary regions (labeled with anti-keratin-5, UEA-1, and AIRE) were fewer and smaller in *Hoil-1^{ΔFoxn1}* mice at day 4 (Fig. 3H–J). Consistent with the flow cytometric analysis, a normal network of K8⁺cTECs was apparent in thymi from neonatal *Hoil-1^{ΔFoxn1}* mice (Fig. 3H). We conclude that HOIL-1 is not required for mTEC differentiation per se but is essential for the expansion and maintenance of all mTEC subpopulations in the perinatal thymus. Furthermore, HOIL-1-mediated signals are not required for the early differentiation and expansion of cTECs yet are required for their maintenance and thymic function later in life (Figs. 1, 2).

HOIL-1 is required to prevent TEC necroptosis to sustain thymic function

To explore how the loss of LUBAC function leads to these outcomes, we performed RNAseq analysis on FACS-purified cTEC and mTEC^{high} from two-week-old *Hoil-1^{lox/lox}* (control) and *Hoil-1^{ΔFoxn1}* mice. We selected this age because: 1) it immediately precedes severe thymic atrophy, therefore the relevant transcriptional changes should be underway, 2) sufficient numbers of TEC could be recovered and 3) the relative expression profiles of the LUBAC components was equivalent to young adult mice (Figure S4A). Visualization of the relationships among the populations in a multidimensional scaling plot showed: [1] that the 3 biological replicates clustered together closely, indicating low experimental variability [2], the first dimension distinguished cTEC from mTEC^{hi}, and [3] the second dimension distinguished the transcriptional impact of *Hoil-1*-deficiency (Fig. 4A). Large transcriptional changes were caused by HOIL loss in cTEC and mTEC^{high}, with ~3,000 and ~5,700 genes reaching the thresholds for statistical significance, although these generally had modest overall expression levels (log expression) or fold changes (Fig. 4B). KEGG pathway analyses of differentially expressed genes revealed enrichment in those associated with cell adhesion, ECM interaction, and various signaling pathways in cTECs, including several metabolic pathways and cell cycle regulators in mTEC^{hi} (Figure S4B, C). Interestingly, we observed enrichment of genes involved in the regulation of cell projection organization and morphology among HOIL-1 induced transcripts in cTEC (Figure S4 D–F); processes recently implicated in thymic regeneration from age-related involution [33].

LUBAC-dependent cell signaling can be required to prevent aberrant cell death via caspase-8-dependent apoptosis and/or by MLKL-dependent necroptosis, depending on the cell type [20–22, 24, 29, 34]. Hierarchical clustering of the transcriptional profiles of genes involved in receptor-mediated programmed cell death was visualized using heatmaps (Fig. 4C). These clearly

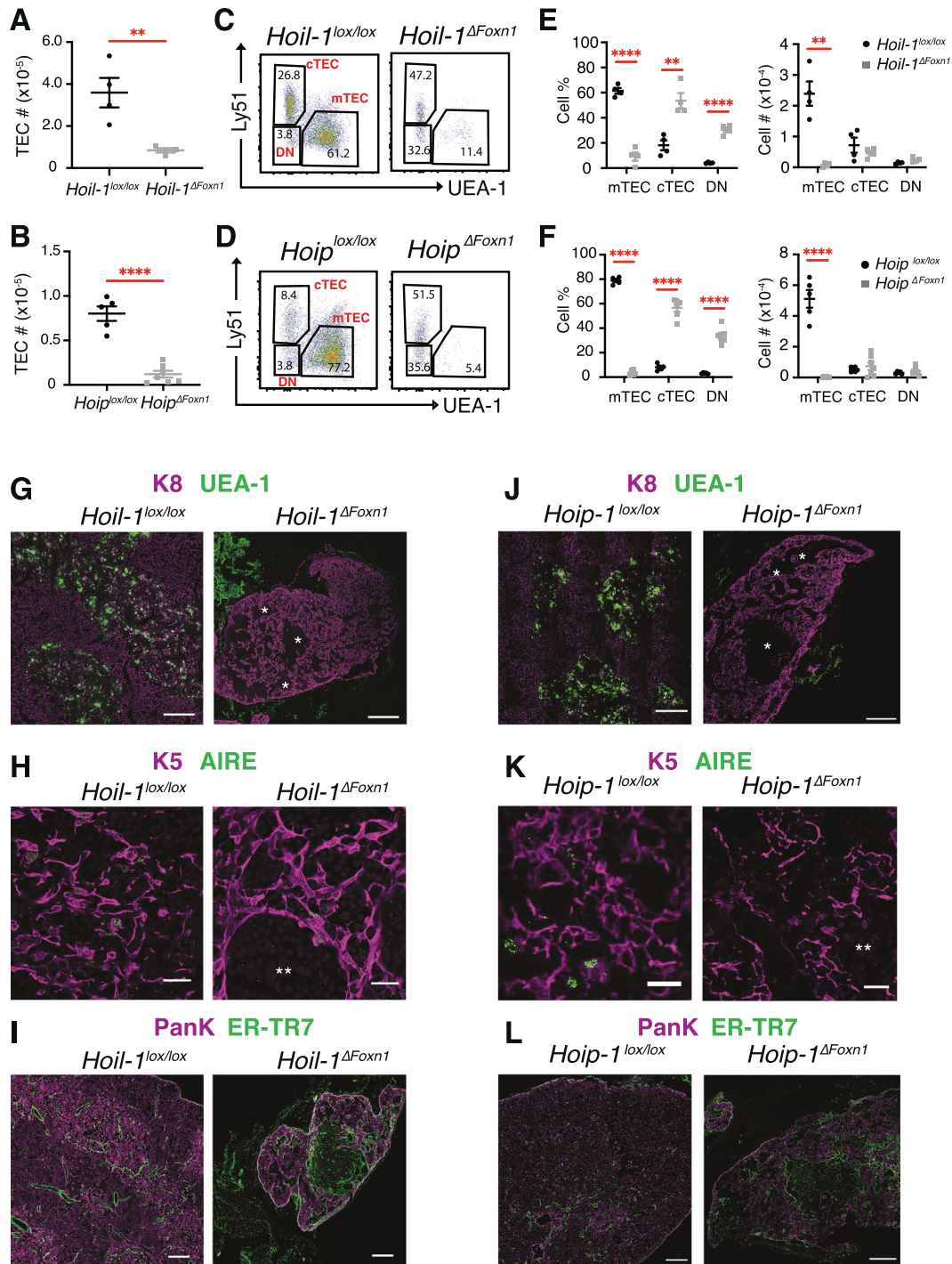


Fig. 2 Loss of TECs and severe disruption of thymic architecture in *Hoil-1^{ΔFoxn1}* and *Hoip^{ΔFoxn1}* mice. TEC (CD45⁺MHCII⁺EpCAM⁺) number from (A) 13-week-old *Hoil-1^{lox/lox}* and *Hoil-1^{ΔFoxn1}* mice or (B) 13-week-old *Hoip^{lox/lox}* and *Hoip^{ΔFoxn1}* mice. Representative flow cytometry plots gated on TECs from (C) 13-week-old *Hoil-1^{lox/lox}* and *Hoil-1^{ΔFoxn1}* mice or (D) 13-week-old *Hoip^{lox/lox}* and *Hoip^{ΔFoxn1}* mice showing Ly51 vs. UEA-1 expression. E, F Mean proportion and number of cTECs (Ly51⁺UEA-1⁻), mTECs (Ly51⁻UEA-1⁺) or “double negative” TECs (Ly51⁻UEA-1⁻) from (E) 13-week-old *Hoil-1^{lox/lox}* and *Hoil-1^{ΔFoxn1}* mice or (F) 13-week-old *Hoip^{lox/lox}* and *Hoip^{ΔFoxn1}* mice. G–L Immunofluorescence images of thymic sections from eight to nine-week-old *Hoil-1^{lox/lox}*, *Hoil-1^{ΔFoxn1}*, *Hoip^{lox/lox}* and *Hoip^{ΔFoxn1}* mice stained with anti-K8 and UEA-1 (G, J), anti-K5 and anti-AIRE (H, K) and ER-TR7 and anti-PanK (I, L). Scale bars represent 200 μ m (G, I, J, L) and 20 μ m (H, K). * and ** represents epithelial cell free regions. Data are representative of at least two independent experiments ($n \geq 3$ /group). Graph bars indicate mean \pm SEM and groups were compared with a Student’s t-test (two sided, unpaired). * $p < 0.05$; ** $p < 0.01$; *** $p < 0.001$; **** $p < 0.0001$.

distinguished TEC subsets from the two genotypes, indicating that substantial differences in this pathway were induced by the loss of HOIL-1 (Fig. 4C). Among these changes, the upregulation of *Mkl1* and *Casp8* was a distinguishing feature of cTECs and mTEC^{high}

cells isolated from 2-week-old *Hoil-1^{ΔFoxn1}* mice. These findings suggest that the loss of HOIL-1 in TECs had sensitized them to MLKL-dependent necroptosis and/or caspase-8-driven apoptosis just prior to the onset of severe thymic atrophy.

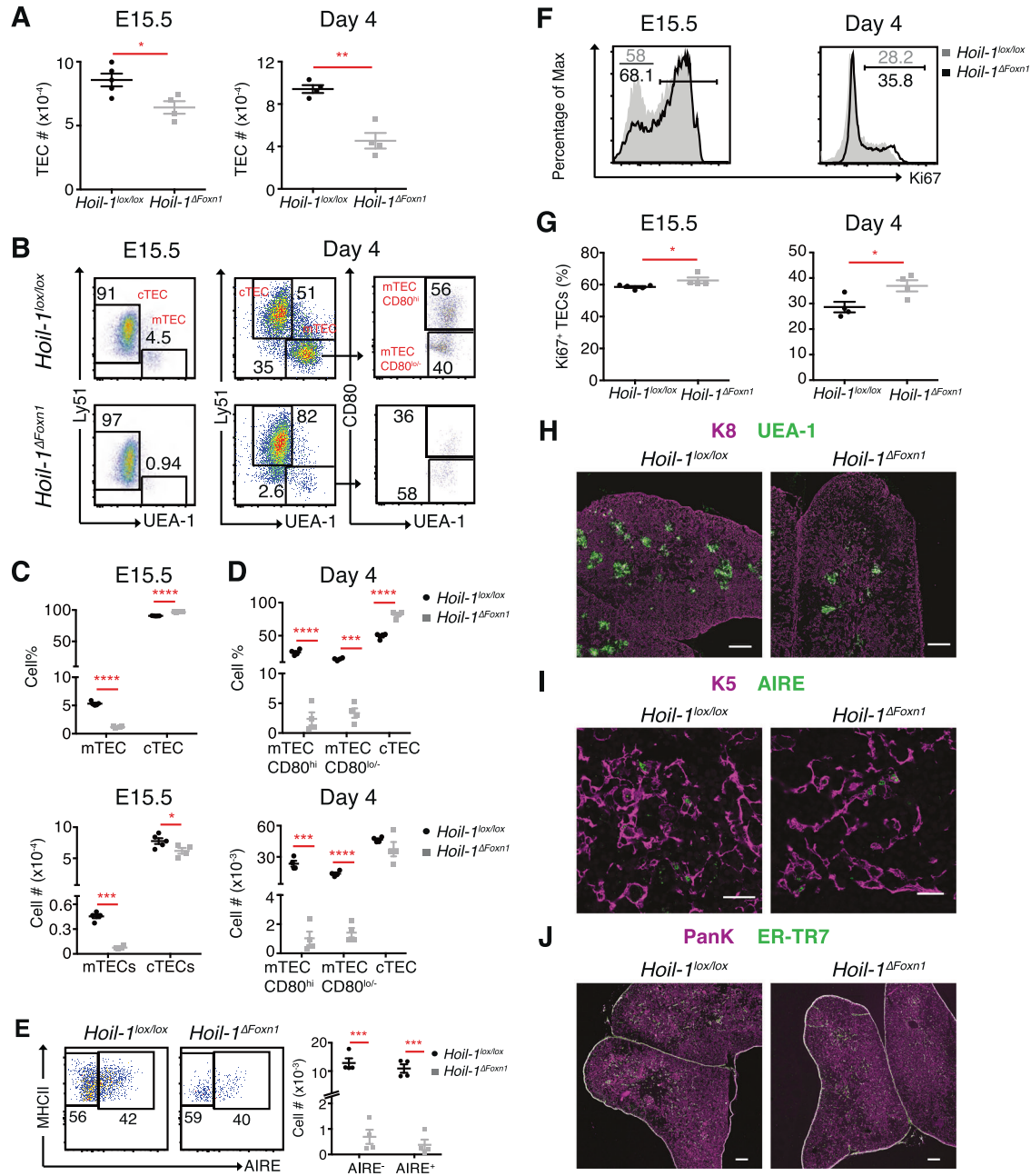
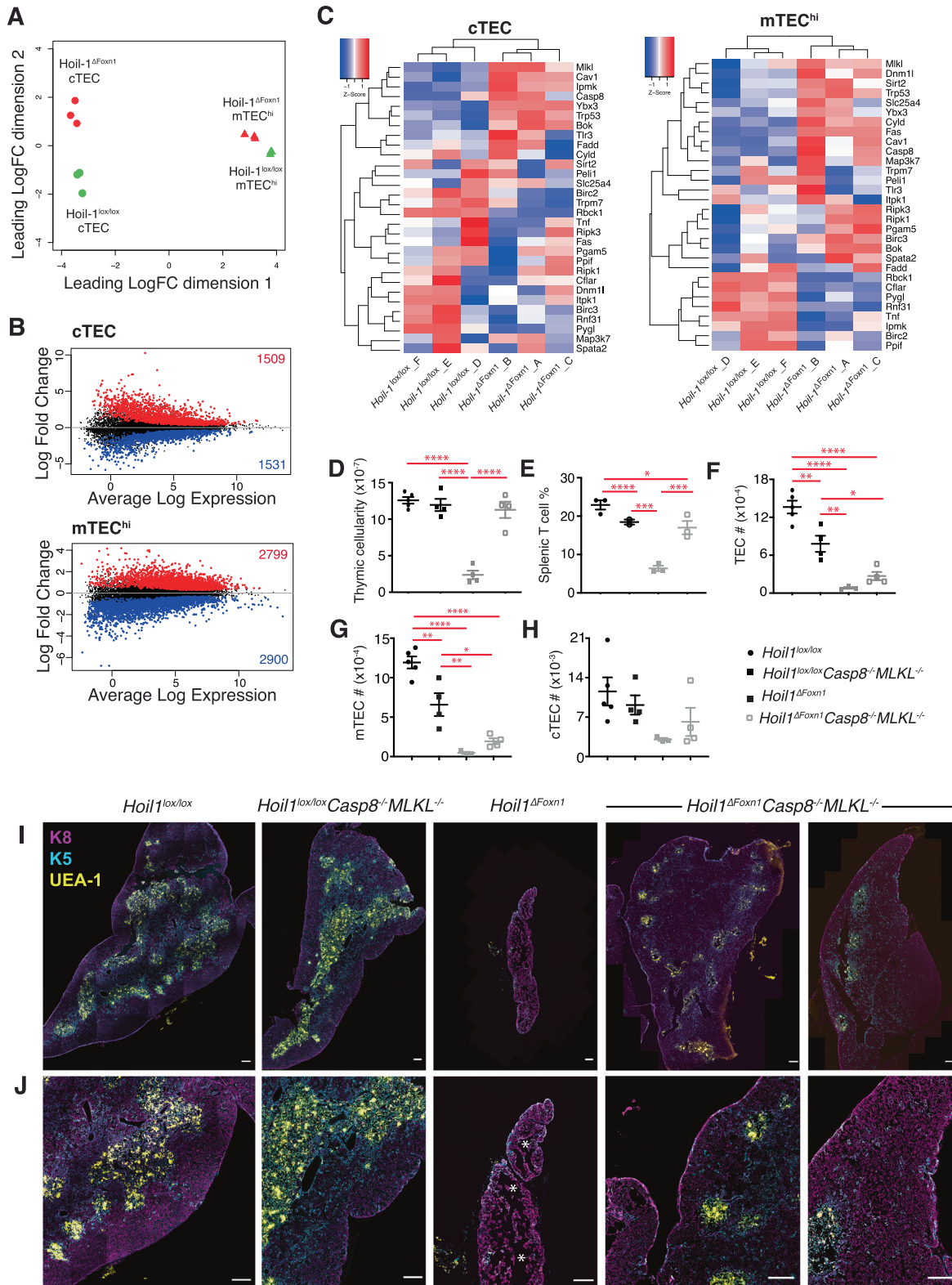


Fig. 3 **HOIL-1 deficiency induces early loss of mTECs in *Hoil-1^{ΔFoxn1}* mice.** **A** TEC (CD45⁻MHCII⁺EpcAM⁺) numbers from E15.5 or four-day-old *Hoil-1^{lox/lox}* and *Hoil-1^{ΔFoxn1}* mice. **B** Representative flow cytometry plots from thymic digests from individual E15.5 or four-day-old *Hoil-1^{lox/lox}* and *Hoil-1^{ΔFoxn1}* mice showing Ly51 vs. UEA-1 gated on TECs (left and middle panels) and CD80 vs. UEA-1 gated on mTECs (right panels). Graphs showing mean proportions (top; of total TEC) and absolute numbers (bottom) of cTECs (Ly51⁺UEA-1⁻) and total mTECs (Ly51⁻UEA-1⁺) from E15.5 (**C**) or cTECs, CD80^{hi} mTECs and CD80^{lo/-} mTECs from four-day-old (**D**) *Hoil-1^{lox/lox}* and *Hoil-1^{ΔFoxn1}* mice. **E** Representative flow cytometry plots of MHC II vs AIRE expression gated on CD80^{hi} mTECs from four-day-old *Hoil-1^{lox/lox}* and *Hoil-1^{ΔFoxn1}* mice and mean cell numbers. **F** Representative histograms and (**G**) graphs showing proportions of proliferating Ki67⁺ TECs. **H–J** Immunofluorescence images of thymic sections from four-day-old *Hoil-1^{lox/lox}* and *Hoil-1^{ΔFoxn1}* mice stained with anti-K8 and UEA-1 (**H**), anti-K5 and AIRE (**I**) and ER-TR7 and anti-PanK (**J**). Scale bars represent 200 μ m (**H, J**) and 20 μ m (**I**). Graph bars indicate mean \pm SEM and experiments with two groups were compared with a Student's t-test (two sided, unpaired).

To test whether the TEC defects observed in HOIL-1-deficient mice were caused by the induction of cell death, we generated *Hoil-1^{ΔFoxn1} Casp8^{-/-} Mkl1^{-/-}* mice in which both apoptotic and necroptotic pathways are non-functional [35]. We first established that young *Casp8^{-/-} Mkl1^{-/-}* mice had normal TN, DP, and SP thymocyte differentiation and splenic T cell homeostasis (Fig. 4D, E, S5), extending on previous analyses [20, 35] and isolating any phenotypes observed in the compound mutants to changes in the TEC

compartment. In striking contrast to the severe thymic atrophy and T cell lymphopenia observed in *Hoil-1^{ΔFoxn1}* mice, *Hoil-1^{ΔFoxn1} Casp8^{-/-} Mkl1^{-/-}* mice had normal thymic cellularity and near-complete restoration of the peripheral T cell population (Fig. 4D, E). This finding indicates that the combined loss of Caspase-8 and MLKL prevented the thymic atrophy observed in adult *Hoil-1^{ΔFoxn1}* mice.

Interestingly, the rescue of thymic function was driven by only partial restoration of the thymic microenvironment. *Hoil-1^{lox/lox}*



lox Casp8^{-/-} Mki1^{-/-} control mice had a reduction in overall TEC number compared to *Hoil-1^{lox/lox}* control mice due to loss of mTEC (Fig. 4F, G). TEC number was further decreased in *Hoil-1^{ΔFoxn1} Casp8^{-/-} Mki1^{-/-}* mice, yet was higher than the atrophied thymus of *Hoil-1^{ΔFoxn1}* mice, suggesting only a portion of TEC were rescued (Fig. 4F). This rescue was accounted for mainly by increased mTEC, although

there was a trend (not statistically significant) towards higher cTEC in *Hoil-1^{ΔFoxn1} Casp8^{-/-} Mki1^{-/-}* compared to *Hoil-1^{ΔFoxn1}* mice (Fig. 4G, H). Immunofluorescent staining of thymic sections from 8-week-old *Hoil-1^{ΔFoxn1} Casp8^{-/-} Mki1^{-/-}* mice confirmed that the rescue of HOIL-1-deficient TEC was partial, demonstrating small, isolated medullary islets composing a reduced area compared to the large, confluent

Fig. 4 HOIL-1 is required to prevent TEC cell death. **A** Multidimensional scaling (MDS) plot of RNAseq data from purified cTECs and mTEC^{hi} from two-week-old *Hoil-1^{lox/lox}* and *Hoil-1^{ΔFoxn1}* mice, taking into account the top 500 most variable genes between a given two samples. **B** Plots of the log-fold changes (*Hoil-1^{ΔFoxn1}*/*Hoil-1^{lox/lox}*) vs average expression for all genes in cTECs (top) and mTEC^{hi} (bottom). Those genes that are significantly upregulated (red) or downregulated (blue) in cell subsets from *Hoil-1^{ΔFoxn1}* mice when compared to *Hoil-1^{lox/lox}* control mice are highlighted. **C** Heatmaps showing the expression of genes involved in necroptosis (GO:0070266) in purified mTEC^{hi} and cTEC subsets. **D** Graph of the mean thymic cellularity in 8-week-old *Hoil-1^{ΔFoxn1}* *Casp8^{-/-}* *Mlkl^{-/-}* mice vs controls. **E** Graph of the proportions of T cells among splenocytes in *Hoil-1^{ΔFoxn1}* *Casp8^{-/-}* *Mlkl^{-/-}* mice vs controls. **F–H** Graph of the total number of TECs (**F**), mTECs (**G**) or cTECs (**H**) recovered from eight-week-old *Hoil-1^{ΔFoxn1}* *Casp8^{-/-}* *Mlkl^{-/-}* mice vs controls. Data are combined from three independent experiments ($n \geq 1-3/\text{group}$). Graph bars indicate mean \pm SEM. **I, J** Immunofluorescence images of thymic sections from 8-week-old *Hoil-1^{lox/lox}* and *Hoil-1^{ΔFoxn1}* *Casp8^{-/-}* *Mlkl^{-/-}* mice stained with anti-K8, anti-K5, and UEA-1 (scale bar = 200 μm).

medulla of thymi from control mice (Fig. 4I, J, S5F). In contrast, a normal, confluent K8⁺ cTEC network and cortical microenvironment were observed (Fig. 4I, J), contrasting the near-complete loss of these cells and regions in *Hoil-1^{ΔFoxn1}* mice (Fig. 2E, F). Therefore, caspase-8 and MLKL deficiency restored the cortical microenvironment and thymic lymphopoiesis in *Hoil-1^{ΔFoxn1}* mice, but only partially restored the thymic medulla.

Collectively, these findings demonstrate that a broad transcriptional program is coordinated in TEC by HOIL-1-mediated signals and that antagonism of TEC necroptosis/apoptosis within this program is a critical mechanism supporting thymic function.

SHARPIN is required for normal mTEC^{low} compartment

The severe thymic atrophy observed in *Hoil-1^{ΔFoxn1}* and *Hoip^{ΔFoxn1}* mice prompted us to also explore the function of the third LUBAC component, SHARPIN, in TECs and thymic function. To circumvent potentially confounding effects of the psoriasis-like inflammatory syndrome in these *Sh^{cpdm/cpdm}* mice [26], we analyzed TECs and thymic function in *Sh^{cpdm/cpdm}* mice prior to the development of dermatitis. Consistent with previous data [20], we recovered normal proportions of DP thymocytes in *Sh^{cpdm/cpdm}* mice, indicating that no stress-related atrophy had occurred. Nevertheless, mild thymic hypotrophy was accompanied by a trend towards lower TEC numbers (Figs. 1B and 5A), with half the normal number of mTEC^{low} in *Sh^{cpdm/cpdm}* mice (Fig. 5B, C). The numbers of cTEC, mTEC^{high}, AIRE⁺TECs, and the proportions of proliferating Ki67⁺ TECs were similar in controls and *Sh^{cpdm/cpdm}* mice (Fig. 5C, S6A, S6B). The observed mTEC^{low} defect was not recapitulated in *Sh^{cpdm/cpdm} → wt* (Ly5.1) hematopoietic chimeras (Figure S6C–F), indicating that the mTEC^{low} defect was a primary consequence of the loss of SHARPIN in the thymic stroma. Analysis of the thymic architecture of *Sharpin^{cpdm/cpdm}* mice revealed mild disruption of the thymic medulla compared to controls, although the location and frequency of AIRE⁺TECs and ERTR7⁺ fibroblasts were comparable to controls (Fig. 5D–F). We conclude that SHARPIN-mediated signals are required specifically to maintain the mTEC^{low} population.

SHARPIN is required to antagonize TNF-induced cell death in certain contexts [10]. This pro-survival activity is not dependent on NF- κ B signaling but involves direct linear ubiquitination of the TNFR1 signaling complex, recruitment of IKK complexes to phosphorylate RIPK1 and prevent caspase-8-mediated apoptosis or RIPK3/MLKL-dependent necroptosis [10, 22–24]. To test whether the loss of mTEC^{low} in *Sh^{cpdm/cpdm}* mice was driven by TNF-induced, caspase-8-dependent apoptosis or RIPK3- and MLKL-dependent necroptosis, we assayed for rescue of the phenotype when these pathways were disabled. Genetic ablation of both caspase-8-driven apoptosis and RIPK3/MLKL-dependent necroptosis in *Sh^{cpdm/cpdm}* *Casp8^{-/-}* *Ripk3^{-/-}* and *Sh^{cpdm/cpdm}* *Casp8^{-/-}* *Mlkl^{-/-}* mice failed to rescue the loss of mTEC^{low} observed in *Sh^{cpdm/cpdm}* mice (Fig. 5G). Consistent with this finding, *Sh^{cpdm/cpdm}* *Tnf^{-/-}* mice also exhibited the loss of mTEC^{low} (Fig. 5H). These data indicate that cell death driven by TNF or other death ligands was not the cause of the mTEC defect in *Sh^{cpdm/cpdm}* mice. Therefore, we conclude that LUBAC deprived of SHARPIN sustains sufficient activity to support TEC survival and thymic function but cannot maintain a normal mTEC^{low} population.

DISCUSSION

The attachment of Met1-linked “linear” chains of ubiquitin to proteins has emerged as a key regulator of NF- κ B and cell death signaling in inflammation, cell survival and differentiation [36]. LUBAC is the only E3 ligase complex known to mediate this form of ubiquitination and it is composed of SHARPIN, HOIL-1 and HOIP. The loss of HOIP or HOIL-1 completely abolishes linear ubiquitination. SHARPIN deficiency only partially reduces this activity, with residual HOIL-1/HOIP complexes sufficient to sustain some LUBAC function in NF- κ B-related programs and the prevention of cell death induced by death ligands other than TNF [10, 12, 14, 21, 22, 25, 34]. Given the critical roles of TNFR family members and NF- κ B signaling in mTEC differentiation and homeostasis [4], we tested the importance of LUBAC function in TECs. Our data highlight essential roles for LUBAC signalling in mTEC development on one hand, and cTEC survival in adulthood on the other.

Conditional ablation of either HOIL-1 or HOIP in TECs greatly diminished all mTEC subsets and the formation of the medulla early in life. This phenotype resembles that observed in mice with compound deficiency in the TNFRSF members RANK plus CD40 or LT β R plus CD40 [7, 9, 37], or those with loss of the NF- κ B signaling proteins NIK, TRAF6 or REL-B, where severe loss of multiple mTEC subpopulations was observed [4]. It is likely that the requirement for the LUBAC for optimal NF- κ B signaling explains the mTEC defects observed in HOIL-1-deficient mice. However, we also found that *Hoil-1^{ΔFoxn1}* mice succumbed to premature thymic atrophy associated with loss of cTEC in adult animals, which appears to be a novel phenotype. These cTEC defects are highly likely to cause the collapse of thymic function, since most thymocyte proliferation is driven by this microenvironment. It is possible that LUBAC signals may be required for an aspect of cTEC function critical to the production of DP thymocytes, the loss of which then feeds back to cause more severe defects in this compartment. Although Shen et al. reported loss of cTEC in young *Nik^{ΔFoxn1}* mice, this phenotype was likely a secondary consequence of the severe autoimmune hepatitis and pneumonitis in these mice, resulting in the stress-induced loss of DP thymocytes [38] required to support this thymic microenvironment. By contrast, *Hoil-1^{ΔFoxn1}* and *Hoip^{ΔFoxn1}* mice were overtly healthy and had no signs of stress-induced DP thymocyte death.

The spontaneous upregulation of genes involved in apoptosis and necroptosis in HOIL-1-deficient TEC hinted that the induction of aberrant cell death might drive their loss; a notion supported by the rescue of the thymic cortex and thymic function in *Hoil-1^{ΔFoxn1}* *Casp8^{-/-}* *Mlkl^{-/-}* mice. This finding is in accord with observations that LUBAC-deficiency in certain cell types can predispose them to TNF-induced apoptosis (which is caspase-8-dependent) or necroptosis (which is RIPK1/RIPK3/MLKL-dependent) [10, 21, 22, 25, 39]. Although our genetic data implicate aberrant cell death in the TEC loss, cortical collapse, and thymic atrophy observed in *Hoil-1^{ΔFoxn1}* mice, only a modest increase in overall TEC number was observed in *Hoil-1^{ΔFoxn1}* *Casp8^{-/-}* *Mlkl^{-/-}* mice, despite restoration of a normal, confluent K8⁺ cTEC network. This observation may reflect a technical limitation of flow cytometric analysis of TEC, whereby the recovery of cTEC greatly underestimates the total number of these cells, as established by

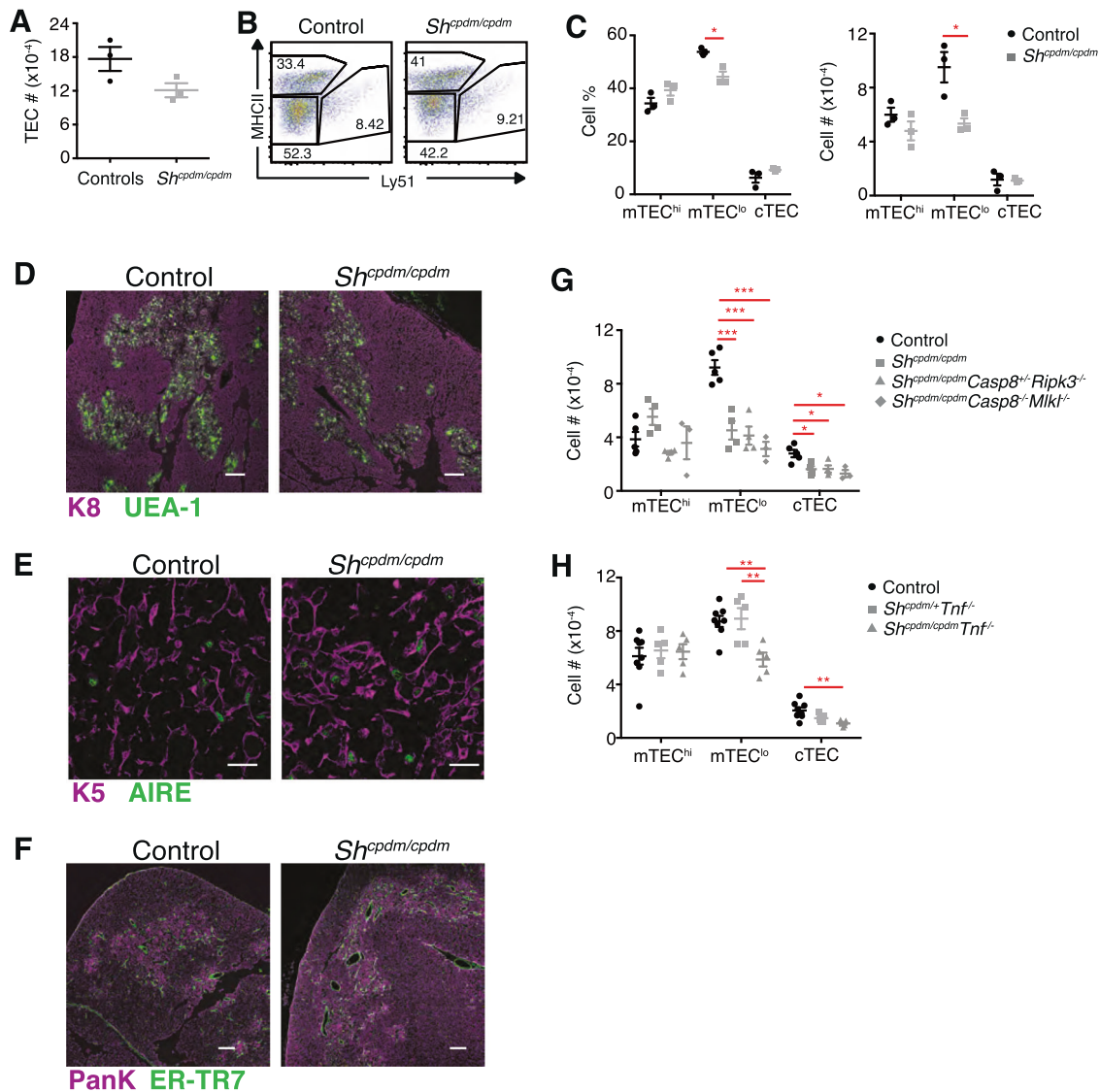


Fig. 5 SHARPIN is required for mTEC^{lo}. **A** TEC (CD45⁺MHCII⁺EpCAM⁺) numbers from six-week-old controls and *cpdm* mice. **B** Representative flow cytometry plots and **(C)** graphs showing proportions and absolute numbers of mTEC^{hi} (MHCII^{hi}Ly51⁻) and mTEC^{lo} mTECs (MHCII^{lo}Ly51⁺) and cTECs (MHCII⁺Ly51⁺). Immunofluorescence images of thymic sections from 6-week-old *Sh^{cpdm/+}* and *Sh^{cpdm/cpdm}* mice stained with **(D)** anti-K8 and UEA-1, **(E)** anti-K5 and AIRE and **(F)** ER-TR7 and anti-PanK. Numbers of **(G)** TEC subsets in *Sh^{cpdm/cpdm}*, *Sh^{cpdm/cpdm} Casp8^{+/-} Ripk3^{-/-}*, *Sh^{cpdm/cpdm} Casp8^{-/-} Mkl^{-/-}*, **(H)** *Sh^{cpdm/+} Tnf^{-/-}*, *Sh^{cpdm/cpdm} Tnf^{-/-}*. Graph bars indicate mean \pm SEM and groups were compared with a Student's t-test (two sided, unpaired). NS not significant * $p < 0.05$; ** $p < 0.01$; *** $p < 0.001$; **** $p < 0.0001$. The control group combines various combinations of genotypes (*Sh^{+/+}*, *Sh^{cpdm/+}*; $n \geq 3$ /group). Scale bars represent 100 μ m (**D**, **F**) and 20 μ m (**E**).

Sakata, et al. [40]. Other approaches will be required to confirm whether loss of LUBAC function primarily impacts cTEC survival in vivo. Alternatively (or in addition), defective regulation of cTEC morphology may influence the atrophy observed in *Hoil-1 Δ Foxn1* mice. We found changes in the expression of genes regulating cellular projections in cTEC from *Hoil-1 Δ Foxn1* mice, reminiscent of features reported in thymic regeneration in aged mice that were independent of cTEC numerical changes [33]. While the precise mechanisms remain to be determined, it is clear that the main lymphopoietic cTEC niches were restored in *Hoil-1 Δ Foxn1 Casp8^{-/-} Mkl^{-/-}* mice, uncovering a critical signaling axis in the cTEC essential for thymic function.

We also found that the restoration of the medulla was not complete in *Hoil-1 Δ Foxn1 Casp8^{-/-} Mkl^{-/-}* mice, therefore it is likely LUBAC modulates other signals supporting TEC expansion and/or survival. In this regard, we note our RNAseq analysis of TEC from

Hoil-1 Δ Foxn1 mice revealed heightened transcription of *Trp53* which, although required for TEC function [41], can also activate cell death and senescence [42]. Future studies will reveal how LUBAC activity intersects with these pathways to impact TEC differentiation, survival, and function.

Consistent with the subordinate role for SHARPIN in linear ubiquitination, thymi from *Sh^{cpdm/cpdm}* mice exhibited milder TEC defects. Although there was a reduction in mTEC^{low} in *Sh^{cpdm/cpdm}* mice compared to controls, all other major TEC subsets were normal. Thus, there appears to be sufficient LUBAC activity in SHARPIN-deficient TEC to support near normal thymic function and homeostasis. Since compound loss of TNF or Caspase-8 plus RIPK3 or Caspase-8 and MLKL did not restore the mTEC^{low} compartment of *Sh^{cpdm/cpdm}* mice, we conclude that the reduced LUBAC activity in *Sh^{cpdm/cpdm}* mice did not predispose these TECs to cell death. Rather, it is likely that SHARPIN is required for the

optimal transduction of NF- κ B signaling, perhaps downstream of CD40/CD40L interactions, which have previously been shown to mediate mTEC^{low} survival and/or expansion [7, 30].

In conclusion, this study defines differential roles for LUBAC components in TECs that correlate with their function in linear ubiquitination. These data reveal dual roles for LUBAC in the development and maintenance of the thymic microenvironment.

METHODS

Mice

The *Sharpin*^{cpdm/cpdm} mutant mouse strain arose on a C57BL/6/Ka background [26] and these mice were backcrossed twice onto a C57BL/6 background [22]. The *Foxn1*^{cre}, *Rnf31*^{lox}, *Rbck1*^{lox}, *Sh*^{cpdm/cpdm}*TNF*^{-/-}, *Sh*^{cpdm/cpdm}*Casp8*^{-/-}*Mkl1*^{-/-} and *Sh*^{cpdm/cpdm}*Casp8*^{+/-}*Ripk3*^{-/-} were generated as previously described [20, 22, 25, 43] and were maintained on a C57BL/6 background. No randomisation or blinding of animals was performed for experiments. All mice were housed under specific pathogen-free housing conditions according to the regulations of the Walter and Eliza Hall Institute of Medical Research.

Thymus digestion

This procedure is described in detail elsewhere; [44] briefly, the two thymic lobes were separated and connective tissue was removed with forceps. Snips were made in each lobe with surgical scissors and the fragments were agitated in 5 mL of RPMI-1640 medium with 25.96 mM HEPES with a wide-bore pipette tip. The supernatant was recovered and replaced by 1 mL of digestion buffer (RPMI-HEPES supplemented with 0.5 Wunsch units Liberase TM (Roche) and DNase I at 0.1% (w/v) (Sigma-Aldrich)). Thymic tissue was then digested at 37 °C for 15 min with gentle agitation after every 5 min. The supernatant was then replaced with 500 μ L of digestion buffer and the digestion incubation was repeated for 15 min. The single-cell suspensions recovered as Fractions 1 and 2 were stained with antibodies to analyze TEC phenotype and number.

Flow cytometry

Single-cell suspensions of lymphoid tissue were stained with various fluorochrome-conjugated antibodies. Surface staining of TECs was performed using the following antibodies that were made at The Walter and Eliza Hall Institute, unless otherwise stated. The TEC lineage depletion cocktail consisted of antibodies against mouse CD16/32 (Fc γ R-block, clone 2.4G2), mouse CD45 PerCP/Cy5.5 (clone 30-F11, Biolegend), mouse CD31 PerCP/Cy5.5 (clone 390, Biolegend) and mouse TER119 PerCP/Cy5.5 (clone TER119, Biolegend). Other conjugates included antibodies to mouse CD326 (EpcAM) APC/Cy7 (clone G8.8, Biolegend), H2-A/E FITC or APC (clone M5/114.15.2), H2-A/E BV421 (clone M5/114.15.2, Biolegend), biotinylated UEA-1 lectin (Vector labs, USA), mouse Ly51 PE or FITC (clone 6C3, Biolegend) and CD80 BV421 (clone 16-10A1, Biolegend). Second step staining with streptavidin PE/Cy7 (BD Biosciences, USA) was used to detect biotinylated UEA1 (Vector Laboratories). Propidium iodide (PI) or DAPI at a final concentration of 2.5 μ g/mL was added to unfixed samples just prior to data acquisition to label dead cells. Intracellular staining with antibodies against human Ki67 FITC (clone MOPC-21, BD Pharmingen) and mouse AIRE FITC (clone 5H12) was performed after fixation and permeabilization using the FoxP3 detection kit (eBioscience). Lymphocytes were stained using antibodies of the following specificities: mouse TCR β PE/Cy7 (H57.59.1, Biolegend), mouse CD4 APC (clone H129), mouse CD4 PerCP/Cy5.5 (GK1.5, Biolegend), mouse CD8 APC/Cy7 or BV650 (clone 53-6.7, Biolegend), mouse CD25 PE or BV510 (clone PC61, Biolegend), mouse CD44 PE or FITC (clone IM781), mouse CD122 PE (clone TM- β 1), mouse CD62L APC/Cy7 (clone MEL-14, Biolegend) and mouse FOXP3 eFluor-450 (clone FJK-165, eBioscience). The immature thymocyte depletion cocktail contained biotinylated antibodies against mouse NK1.1 (clone PK136, Biolegend), TER119 (TER119), GR1 (clone RB6-8C5), Mac-1 (clone M1-170), and B220 (RA3-6B2), and they were detected with streptavidin BV786 (Biolegend). Screening of TCRV β repertoire in the CD4⁺ and CD8⁺ populations was performed with the mouse V β TCR Screening Panel (BD Pharmingen). Samples were acquired using Fortessa X20 (BD Biosciences) and LSR II analysers (BD Bioscience) and data analyzed using FlowJo software 9.9 (TreeStar).

PCR

The floxed allele (in the absence of Cre) in sorted TECs (CD45⁻MHCII⁺EpcAM⁺), stromal cells (CD45⁺EpcAM⁻) and hematopoietic cells (CD45⁺EpcAM⁻)

from 3–4 week-old *Hoil-1*^{lox/lox} and *Hoil-1* ^{Δ Foxn1} mice was detected by using *Hoil-1*-Fwd 5'-ACC CTA GGC CTA GTC AGT GCA AA-3' with *Hoil-1*-Rev-5'-AGG CTG TGG TCC ATT CTA GCC AT-3' producing 580 bp band. The conditions were: 96 °C 2 min; 30 cycles for 96 °C 20 s, 57 °C 20 s, 72 °C 1 min 20 s and final extension of 72 °C 5 min. The deleted allele (after Cre-mediated recombination) was detected by using Fwd 5'-ATG GTC TAC AGA AGA AAG GC-3' and Rev 5'-GGG AGA TTC AGA CAA GGT TTC-3' producing 581 bp. The conditions were: 94 °C 4 min; 30 cycles for 94 °C 40 s, 55 °C 30 s, 72 °C 1 min and final extension of 72 °C 5 min.

Immunohistology

Thymi from adult (8 weeks) and neonatal (day 4) mice were isolated, embedded in Tissue-Tek O.C.T compound (Sakura Finetek, U.S.A.) and snap-frozen in a liquid nitrogen/isopentane slurry. Sections of 5–8 μ m were cut using a Microm HM550 Cryostat (Thermo Scientific). Sections were fixed in ice cold acetone (Merck) for 3 min and air-dried for 2 min. Sections were blocked with 5% (v/v) goat serum in PBS with 0.1% Tween-20 (v/v) for 30 min at room temperature before incubation with primary antibodies for 30 min. Primary antibodies of the following specificities were used: mouse K5 (Covance, clone Poly 19055), biotinylated mouse pan-keratin (LifeSpan BioSciences, clone Lu-5), biotinylated UEA-1 lectin (Vector labs, USA), mouse AIRE-Alexa647 (clone 5H12), mouse K8 (clone Troma-1, DSHB) and ER-TR7 (provided by Prof Richard Boyd, Monash University). Following three 5 min washes in PBS, sections were incubated with appropriate secondary reagents (antibodies or streptavidin) conjugated to fluorochromes (anti-rabbit IgG Alexa-555 (Life Technologies) and streptavidin FITC (Invitrogen)) for 30 min, counterstained with DAPI (Sigma-Aldrich), then mounted with Vectashield (Vector labs). Images were collected using a LSM780 confocal microscope with Zen 2012 SP2 (black) software v11.0 (Zeiss). Single optical sections and maximal intensity projection images were processed for presentation using OMERO [45] or ImageJ (2.0.0). For quantification of medullary area, 1 of 40 neighbouring sections, or every one of 20 for thymic from adult *Hoil-1* ^{Δ Foxn1} mice, were selected as a representative section, stained with UEA-1(40) and processed using ImageJ (2.0.0).

RNA sequencing

Thymi were pooled from eight- or two-week-old WT mice and digested to isolate TECs (CD45⁺MHCII⁺EpcAM⁺) (44). At the end of the digestion, fractions were pooled, enriched and purified using anti-mouse CD45 microbeads (Miltenyi Biotec, Germany, Cat # 130052301) and FACS ARIA (BD). Cell pellets were snap-frozen on dry ice and stored at -80 °C. RNA was isolated using the miRNeasy Micro Kit (Qiagen) with on column DNase digestion according to the manufacturer's instructions. First strand cDNA synthesis and cDNA amplification were performed using the SMART-Seq[®] v4 Ultra[®] Low Input RNA Kit for Sequencing (Clontech Laboratories) according to the manufacturer's instructions. Complementary DNA (cDNA) libraries were prepared and indexed separately using the Nextera[®] XT DNA Library Preparation Kit (Illumina) following the manufacturer's instructions. Each indexed cDNA sample library was quantified using the Agilent TAPPE station and the Qubit[™] DNA BR assay kit for Qubit 3.0[®] Fluorometer (Life technologies). The indexed sample libraries were pooled and diluted to 1.5 pM for 75 base paired-end sequencing on a NextSeq 500 instrument using the v2 150 cycle High Output kit (Illumina) according to the manufacturer's instructions.

Between 13 and 35 million read pairs were generated for each sample and reads were aligned to the *Mus musculus* genome (mm10) using Rsubread [46]. The number of read pairs overlapping mouse Entrez genes was summarized using featureCounts and Rsubread's built-in NCBI gene annotation. Low expressed genes were filtered out using edgeR's filterByExpr function [47]. Genes without current annotation were also filtered. Differential expression (DE) analyses were undertaken using the edgeR and limma [48] software packages. Library sizes were normalized using the trimmed mean of M-values (TMM) method [49]. Sample quality weights were estimated using voomWithQualityWeights [50] and differential expression was evaluated using voom [51] with robust empirical Bayes estimation of the variances [52]. Correlations between repeated measurements from the same mouse were estimated using the duplicateCorrelation method [53]. The false discovery rate (FDR) was controlled below 0.05 using the method of Benjamini and Hochberg. Overrepresentation of Gene Ontology (GO) terms and KEGG pathways for the differentially expressed genes were identified using limma's goana and kegg functions. Barcode plots illustrating the cross correlations between the cell types, and enrichment of interested pathway genes were drawn

using limma's barcodeplot function. Gene set enrichment tests used the roast method [54]. Heatmaps were drawn using limma's coolmap function. Sequence data that support the findings of this study have been deposited with GEO with the primary accession code GSE139898.

Hematopoietic reconstitution experiments

Bone marrow reconstitution experiments were performed using recipient WT (C57BL/6-Ly5.1) mice irradiated with 2×550 RAD and reconstituted within 24 h by intravenous injection with 5×10^6 of BM cells from donors of interest (all on a C57BL/6-Ly5.2 background). Reconstituted mice were analyzed 6.5 weeks after reconstitution.

Data analysis

Statistical analyses were performed using Prism version 7. Experiments containing three or more groups were analyzed using ANOVA followed by a Tukey's post-hoc test. Experiments with two groups were analyzed with two-tailed Student's *t*-test. *P* values < 0.05 were considered as the threshold for statistical significance for all statistical tests.

REFERENCES

- Petrie HT, Zuniga-Pflucker JC. Zoned out: functional mapping of stromal signaling microenvironments in the thymus. *Annu Rev Immunol* 2007;25:649–79.
- Klein L, Kyewski B, Allen PM, Hogquist KA. Positive and negative selection of the T cell repertoire: what thymocytes see (and don't see). *Nat Rev Immunol* 2014;14:377–91.
- Takaba H, Morishita Y, Tomofuji Y, Danks L, Nitta T, Komatsu N, et al. Fezf2 orchestrates a thymic program of self-antigen expression for immune tolerance. *Cell* 2015;163:975–87.
- Abramson J, Anderson G. Thymic Epithelial Cells. *Annu Rev Immunol* 2017;35:85–118.
- Cosway EJ, Lucas B, James KD, Parnell SM, Carvalho-Gaspar M, White AJ, et al. Redefining thymus medulla specialization for central tolerance. *J Exp Med* 2017;214:3183–95.
- Sun SC. The non-canonical NF- κ B pathway in immunity and inflammation. *Nat Rev Immunol* 2017;17:545–58.
- Akiyama T, Shimo Y, Yanai H, Qin J, Ohshima D, Maruyama Y, et al. The tumor necrosis factor family receptors RANK and CD40 cooperatively establish the thymic medullary microenvironment and self-tolerance. *Immunity* 2008;29:423–37.
- Desanti GE, Cowan JE, Baik S, Parnell SM, White AJ, Penninger JM, et al. Developmentally regulated availability of RANKL and CD40 ligand reveals distinct mechanisms of fetal and adult cross-talk in the thymus medulla. *J Immunol* 2012;189:5519–26.
- Hikosaka Y, Nitta T, Ohigashi I, Yano K, Ishimaru N, Hayashi Y, et al. The cytokine RANKL produced by positively selected thymocytes fosters medullary thymic epithelial cells that express autoimmune regulator. *Immunity* 2008;29:438–50.
- Gerlach B, Cordier SM, Schmukle AC, Emmerich CH, Rieser E, Haas TL, et al. Linear ubiquitination prevents inflammation and regulates immune signalling. *Nature* 2011;471:591–6.
- Haas TL, Emmerich CH, Gerlach B, Schmukle AC, Cordier SM, Rieser E, et al. Recruitment of the linear ubiquitin chain assembly complex stabilizes the TNF-R1 signaling complex and is required for TNF-mediated gene induction. *Mol Cell* 2009;36:831–44.
- Tokunaga F, Nakagawa T, Nakahara M, Saeki Y, Taniguchi M, Sakata S, et al. SHARPIN is a component of the NF- κ B-activating linear ubiquitin chain assembly complex. *Nature* 2011;471:633–6.
- Draber P, Kupka S, Reichert M, Draberova H, Lafont E, de Miguel D, et al. LUBAC-Recruited CYLD and A20 Regulate Gene Activation and Cell Death by Exerting Opposing Effects on Linear Ubiquitin in Signaling Complexes. *Cell Rep* 2015;13:2258–72.
- Ikeda F, Deribe YL, Skanland SS, Stieglitz B, Grabbe C, Franz-Wachtel M, et al. SHARPIN forms a linear ubiquitin ligase complex regulating NF- κ B activity and apoptosis. *Nature* 2011;471:637–41.
- Kirisako T, Kamei K, Murata S, Kato M, Fukumoto H, Kanie M, et al. A ubiquitin ligase complex assembles linear polyubiquitin chains. *EMBO J* 2006;25:4877–87.
- Yamanaka K, Ishikawa H, Megumi Y, Tokunaga F, Kanie M, Rouault TA, et al. Identification of the ubiquitin-protein ligase that recognizes oxidized IRP2. *Nat Cell Biol* 2003;5:336–40.
- Boisson B, Laplantine E, Dobbs K, Cobat A, Tarantino N, Hazen M, et al. Human HOIP and LUBAC deficiency underlies autoinflammation, immunodeficiency, amylopectinosis, and lymphangiectasia. *J Exp Med* 2015;212:939–51.
- Boisson B, Laplantine E, Prando C, Giliani S, Israelsson E, Xu Z, et al. Immunodeficiency, autoinflammation and amylopectinosis in humans with inherited HOIL-1 and LUBAC deficiency. *Nat Immunol* 2012;13:1178–86.
- Liang Y, Seymour RE, Sundberg JP. Inhibition of NF- κ B signaling retards eosinophilic dermatitis in SHARPIN-deficient mice. *J Invest Dermatol* 2011;131:141–9.
- Teh CE, Lalaoui N, Jain R, Policheni AN, Heinlein M, Alvarez-Diaz S, et al. Linear ubiquitin chain assembly complex coordinates late thymic T-cell differentiation and regulatory T-cell homeostasis. *Nat Commun* 2016;7:13353.
- Peltzer N, Darding M, Montinaro A, Draber P, Draberova H, Kupka S, et al. LUBAC is essential for embryogenesis by preventing cell death and enabling haematopoiesis. *Nature* 2018;557:112–7.
- Rickard JA, Anderton H, Emami N, Nachbur U, Darding M, Peltzer N, et al. TNFR1-dependent cell death drives inflammation in Sharpin-deficient mice. *Elife* 2014;3:e03464.
- Kumari S, Redouane Y, Lopez-Mosqueda J, Shiraishi R, Romanowska M, Lutzmayer S, et al. Sharpin prevents skin inflammation by inhibiting TNFR1-induced keratinocyte apoptosis. *Elife* 2014;3:e03422.
- Lafont E, Draber P, Rieser E, Reichert M, Kupka S, de Miguel D, et al. TBK1 and IKKepsilon prevent TNF-induced cell death by RIPK1 phosphorylation. *Nat Cell Biol* 2018;20:1389–99.
- Peltzer N, Rieser E, Taraborrelli L, Draber P, Darding M, Pernaute B, et al. HOIP deficiency causes embryonic lethality by aberrant TNFR1-mediated endothelial cell death. *Cell Rep* 2014;9:153–65.
- Hogenesch H, Gijbels MJ, Offerman E, van Hooft J, van Bekkum DW, Zurcher C. A spontaneous mutation characterized by chronic proliferative dermatitis in C57BL mice. *Am J Pathol* 1993;143:972–82.
- Seymour RE, Hasham MG, Cox GA, Shultz LD, Hogenesch H, Roopenian DC, et al. Spontaneous mutations in the mouse Sharpin gene result in multiorgan inflammation, immune system dysregulation and dermatitis. *Genes Immun* 2007;8:416–21.
- Park Y, Jin HS, Lopez J, Lee J, Liao L, Elly C, et al. SHARPIN controls regulatory T cells by negatively modulating the T cell antigen receptor complex. *Nat Immunol* 2016;17:286–96.
- Webb LV, Barbarulo A, Huysentruyt J, Vanden Berghe T, Takahashi N, Ley S, et al. Survival of single positive thymocytes depends upon developmental control of RIPK1 kinase signaling by the IKK complex independent of NF- κ B. *Immunity* 2019;50:348–61 e4.
- Gray DH, Seach N, Ueno T, Milton MK, Liston A, Lew AM, et al. Developmental kinetics, turnover, and stimulatory capacity of thymic epithelial cells. *Blood* 2006;108:3777–85.
- Williams JA, Zhang J, Jeon H, Nitta T, Ohigashi I, Klug D, et al. Thymic medullary epithelium and thymocyte self-tolerance require cooperation between CD28-CD80/86 and CD40-CD40L costimulatory pathways. *J Immunol* 2014;192:630–40.
- den Braber I, Mugwagwa T, Vrisekoop N, Westera L, Mogling R, de Boer AB, et al. Maintenance of peripheral naive T cells is sustained by thymus output in mice but not humans. *Immunity* 2012;36:288–97.
- Venables T, Griffith AV, DeAraujo A, Petrie HT. Dynamic changes in epithelial cell morphology control thymic organ size during atrophy and regeneration. *Nat Commun* 2019;10:4402.
- Taraborrelli L, Peltzer N, Montinaro A, Kupka S, Rieser E, Hartwig T, et al. LUBAC prevents lethal dermatitis by inhibiting cell death induced by TNF, TRAIL and CD95L. *Nat Commun* 2018;9:3910.
- Alvarez-Diaz S, Dillon CP, Lalaoui N, Tanzer MC, Rodriguez DA, Lin A, et al. The pseudokinase MLKL and the kinase RIPK3 have distinct roles in autoimmune disease caused by loss of death-receptor-induced apoptosis. *Immunity* 2016;45:513–26.
- Peltzer N, Walczak H. Cell death and inflammation - a vital but dangerous liaison. *Trends Immunol* 2019;40:387–402.
- Jenkinson SR, Williams JA, Jeon H, Zhang J, Nitta T, Ohigashi I, et al. TRAF3 enforces the requirement for T cell cross-talk in thymic medullary epithelial development. *Proc Natl Acad Sci Usa* 2013;110:21107–12.
- Shen H, Ji Y, Xiong Y, Kim H, Zhong X, Jin MG, et al. Medullary thymic epithelial NF- κ B-inducing kinase (NIK)/IKKalpha pathway shapes autoimmunity and liver and lung homeostasis in mice. *Proc Natl Acad Sci Usa* 2019;116:19090–7.
- Shimizu Y, Taraborrelli L, Walczak H. Linear ubiquitination in immunity. *Immunol Rev* 2015;266:190–207.
- Sakata M, Ohigashi I, Takahama Y. Cellularity of thymic epithelial cells in the postnatal mouse. *J Immunol* 2018;200:1382–8.
- Rodrigues PM, Ribeiro AR, Perrod C, Landry JJM, Araujo L, Pereira-Castro I, et al. Thymic epithelial cells require p53 to support their long-term function in thymopoiesis in mice. *Blood* 2017;130:478–88.
- Aubrey BJ, Kelly GL, Janic A, Herold MJ, Strasser A. How does p53 induce apoptosis and how does this relate to p53-mediated tumour suppression? *Cell Death Differ* 2018;25:104–13.
- Zuklys S, Gill J, Keller MP, Hauri-Hohl N, Zhanybekova S, Balciunaite G, et al. Stabilized beta-catenin in thymic epithelial cells blocks thymus development and function. *J Immunol* 2009;182:2997–3007.

44. Jain R, Gray DH. Isolation of thymic epithelial cells and analysis by flow cytometry. *Curr Protoc Immunol*. 2014;107:3.26.1–3.26.15. <https://doi.org/10.1002/0471142735.im0326s107>.
45. Allan C, Burel JM, Moore J, Blackburn C, Linkert M, Loynton S, et al. OMERO: flexible, model-driven data management for experimental biology. *Nat Methods* 2012;9:245–53.
46. Liao Y, Smyth GK, Shi W. The R package Rsubread is easier, faster, cheaper and better for alignment and quantification of RNA sequencing reads. *Nucleic Acids Res* 2019;47:e47.
47. Chen Y, Lun AT, Smyth GK. From reads to genes to pathways: differential expression analysis of RNA-Seq experiments using Rsubread and the edgeR quasi-likelihood pipeline. *F1000Res* 2016;5:1438.
48. Ritchie ME, Phipson B, Wu D, Hu Y, Law CW, Shi W, et al. limma powers differential expression analysis for RNA-sequencing and microarray studies. *Nucleic Acids Res* 2015;43:e47.
49. Robinson MD, Oshlack A. A scaling normalization method for differential expression analysis of RNA-seq data. *Genome Biol* 2010;11:R25.
50. Liu R, Holik AZ, Su S, Jansz N, Chen K, Leong HS, et al. Why weight? Modelling sample and observational level variability improves power in RNA-seq analyses. *Nucleic Acids Res* 2015;43:e97.
51. Law CW, Chen Y, Shi W, Smyth GK. voom: Precision weights unlock linear model analysis tools for RNA-seq read counts. *Genome Biol* 2014;15:R29.
52. Phipson B, Lee S, Majewski IJ, Alexander WS, Smyth GK. Robust Hyperparameter Estimation Protects against Hypervariable Genes and Improves Power to Detect Differential Expression. *Ann Appl Stat* 2016;10:946–63.
53. Smyth GK, Michaud J, Scott HS. Use of within-array replicate spots for assessing differential expression in microarray experiments. *Bioinformatics* 2005;21:2067–75.
54. Wu D, Lim E, Vaillant F, Asselin-Labat ML, Visvader JE, Smyth GK. ROAST: rotation gene set tests for complex microarray experiments. *Bioinformatics* 2010;26:2176–82.

ACKNOWLEDGEMENTS

We gratefully acknowledge the Gray, Strasser and Herold laboratories and Dr Nieves Peltzer for valuable feedback on this study. We thank the WEHI Flow Cytometry Laboratory and the Center for Dynamic Imaging; B Helbert, K Mackwell, C Young for mouse genotyping; G Siciliano, H Marks, K Humphreys and S O'Connor for animal husbandry; and L Tai for technical assistance. TROMA-I was deposited to the DSHB by Brulet, P./Kemler, R. (DSHB Hybridoma Product TROMA-I).

AUTHOR CONTRIBUTIONS

Conceptualization, RJ, AS and DHDG; Methodology, RJ, JMS, KZ, AS and DHDG; Investigation, RJ, JMS, MH, WA, KZ, FK and DHDG; Resources, PB, CH, JR, HW, JS, AS,

DHDG; Writing - Original draft, RJ, JMS, and DHDG; Writing—Review and editing, RJ, JMS, MH, KZ, AS, HW, JS and DHDG. The authors declare no conflict of interest. Correspondence and requests for materials should be addressed to DHDG.

FUNDING

This work was supported by grants GNT0637353, GNT1049724, GNT1187367, GNT1025594 and GNT1121325, and Fellowships 1090236 and 1158024 (for DHDG), Principle Research Fellowship 1016701 (for JS), Senior Principal Research Fellowship 1020363 (for AS) from the Australian National Health and Medical Research Council and the Leukaemia Research Foundation. RJ was supported by MIRS and MIFRS from the University of Melbourne. H.W. is supported by an Alexander von Humboldt Professorship Award, a Wellcome Trust Investigator Award (214342/Z/18/Z), a Cancer Research UK programme grant (A27323), a Medical Research Council UK Grant (MR/S00811X/1) and by the German Research Foundation (DFG) in the context of SFB 1399 and SFB 1403. This work was made possible through Victorian State Government Operational Infrastructure Support and Australian Government NHMRC IRIISS.

COMPETING INTERESTS

The authors declare no competing interests.

ETHICS

All animal work in this study was performed in accordance with the ethical regulations of the Walter and Eliza Hall Institute of Medical Research.

ADDITIONAL INFORMATION

Supplementary information The online version contains supplementary material available at <https://doi.org/10.1038/s41418-021-00850-8>.

Correspondence and requests for materials should be addressed to D.H.D.G.

Reprints and permission information is available at <http://www.nature.com/reprints>

Publisher's note Springer Nature remains neutral with regard to jurisdictional claims in published maps and institutional affiliations.